

CFD KINETIC SCHEME VALIDATION FOR LIQUID ROCKET ENGINE FUELLED BY OXYGEN/METHANE

*Pasquale Natale**, *Guido Saccone*** and *Francesco Battista****

** Centro Italiano Ricerche Aerospaziali*

Via Maiorise, 81043 Capua (CE), Italy, p.natale@cira.it

***Centro Italiano Ricerche Aerospaziali*

Via Maiorise, 81043 Capua (CE), Italy, g.saccone@cira.it

****Centro Italiano Ricerche Aerospaziali*

Via Maiorise, 81043 Capua (CE), Italy, f.battista@cira.it

Abstract

In recent years, greater attention has been paid to green propellants, among those liquid methane is one of the most promising choice. This has also been encouraged by the abolition of hydrazine for its intrinsic human-rating concerns. On the other hand, the adoption of methane as a fuel introduces some issues about modelling. Detailed kinetic schemes are required to properly reconstruct combustion process. This is especially true for rocket propulsion problems, in which the combustion is characterized by high pressure and not stoichiometric mixture ratio. Moreover, detailed scheme may not be feasible for CFD applications, due to high computational cost. For this reason, adoption of reduced schemes is encouraged, even if detailed mechanism description is required. In the present work, a reduced kinetic scheme (HPRB, by CIRA) will be presented for a specific LRE application. Some experimental firing-tests (i.e. FSBB test-campaign) will then be compared with model results, in order to validate the proposed model.

1. Introduction

Traditionally, high performance rocket engines have used LO_x and hydrogen or LO_x and kerosene, while, as such, methane has not yet been used in a commercial launch vehicle. Nevertheless, several LO_x /methane engines have been built and/or under development. Methane exhibits peculiar thermodynamic properties in typical operative range: it has a high specific heat, useful for cooling purposes; it has a high critical temperature, which leads to higher storage temperature (thus, lighter thermal insulation systems); it has a relatively high density, which allows the use of smaller tanks (thus, lighter structures). Hereinafter, a short, not exhaustive, list of projects in which methane has been selected as fuel:

- MIRA (Avio KBKha Khrunichev Progres Kuznetsov) cryogenic LO_x /liquid methane upperstage replacing both Zefiro 9 and AVUM.
- XCOR along with Alliant Techsystems Inc. (ARK) built a 33kN LO_x /methane regenerative cooled engine as part of NASA's Exploration Technology Development Program (XR5M15 in Figure 1).
- A Purdue University student team has designed, built, and tested a liquid LO_x /Methane thrust chamber as part of NASA's Project Morpheus. In this case, the thrust chamber has the ability to "throttle". It is designed and tested for automated landing systems.
- Aerojet developed a LO_x /Methane reaction engine based on their previous LO_x /Ethanol engines, and a 24.5 kN main engine for lunar lander ascents (Figure 2).
- RAPTOR is a staged combustion, methane-fuelled rocket engine under development by SpaceX. The engines are powered by cryogenic liquid methane and liquid oxygen (LO_x), rather than the RP-1 kerosene and LO_x used in all previous SpaceX Falcon rockets which use or used Merlin 1A, 1C, & 1D and Kestrel engines. The Raptor

engine will have about twice the thrust of the Merlin 1D engine that powers the current Falcon 9 launch vehicle. With its almost 2 MN of thrust, it is the most powerful methane-fuelled LRE.



Figure 1: XCOR test firing of a 33kN LOX/methane engine



Figure 2: Aerojet 100-lbf LOX/LCH4 reaction control engine in test at NASA GRC

All of these projects, and others not mentioned, justify the effort of studying methane/oxygen combustion. In order to use CFD as a reliable tool for verifying design of LRE, it is necessary to set up reaction model in the specific application.

1.1. HYPROB-NEW project

In the framework of HYPROB-NEW project, also CIRA is carrying out a LOx/methane LRE development [1]. Among others, FSBB bread-board was designed, developed and tested in order to validate the injector head design [2]. This breadboard is a full replica of a final demonstrator (DEMO, Figure 3) except for cooling system. In fact, for the FSBB the cooling system has been structurally reinforced in order to prevent possible injector head failure and it is fed by demi-water, in place of liquid methane. In this way, it is possible to study injection head behaviour without the complication of the regenerative cooling issue combustion. Moreover, the use of water allows for higher design margins since it has a high specific heat and it exhibits properties relatively less sensitive to temperature and pressure changes. Very high heat fluxes are related to the combustion (order of tens of MW/m^2). Thus, in order to have a robust and reliable cooling system, it is mandatory to know the entire combustion process well, keeping CFD runtime feasible for design purposes. The objective of this work is to introduce a kinetic scheme that responds to all of these requirements and present a preliminary validation stage obtained comparing CFD results with experimental data acquired during FSBB test-campaign.



Figure 3: Sketch view of HYPROB DEMO test-article.

2. Combustion Models for CFD simulations

When dealing with these problems, *chemical equilibrium* cannot be considered as a valid hypothesis. Indeed, evaluation of the Damköhler number confirms us that flow time scale is comparable to the chemical one. For this reason, in order to predict the actual gas composition, it is necessary to describe all the steps during the reaction. The pressure reached inside the combustion chamber and the adiabatic flame temperature depend on the gas composition, therefore they represent a key point of the CFD analysis. In fact, the overall system performance (thrust) depends on the chamber pressure and the design of cooling systems is affected by the chamber temperature.

For all these reasons, the adoption of a detailed kinetic scheme is highly appreciated, while mono-step and dual-step global schemes are inappropriate.

Many CFD solvers, and also Ansys Fluent® (adopted in this work), can model the mixing and transport of chemical species by integrating conservation equations describing convection, diffusion, and reaction sources for each component species. Multiple simultaneous chemical reactions occurring in the bulk phase (volumetric reactions) can be modelled. In this work only volumetric reactions will be considered.

The species transport is governed by the following general conservation equation:

$$\frac{\partial}{\partial t}(\rho Y_i) + \nabla \cdot (\rho \vec{v} Y_i) = -\nabla \cdot \vec{J}_i + R_i + S_i \quad (1)$$

Where: Y_i is the local mass fraction of species i , R_i is the net rate of production of species i , S_i is the rate of creation. These reaction rates, which appear on the right hand, can be computed by one of the three turbulence combustion models.

2.1. Laminar Finite-Rate Model

In this model, the effects of turbulent fluctuations are ignored, and reaction rates are determined by Arrhenius kinetic expressions. The model is suitable for laminar flames, but it is generally inaccurate for turbulent flames due to non-linear Arrhenius chemical kinetics. In other words, LFR model should be adopted when convective mass transport rate is much more important than reaction rate. Since the first Damköhler number is represented by the ratio between the flow time scale and the chemical one, it can be asserted that LFR model is highly recommended when $Da < 1000$.

In the study case, LFR model is not recommended for combustion chamber, where the flow is characterized by high turbulence and low convective transport, while is it appropriate for supersonic exhausts, where convective transport prevails.

Using LRF model it is possible to define the chemical kinetic scheme in order to obtain the product mixture starting from the reactants.

2.2. Eddy-Dissipation Model

When the combustion is extremely fast, the overall rate of reactions is controlled only by turbulent mixing. In such cases, the combustion is said to be mixing-limited, and the complex (and often unknown) chemical kinetic rates can be safely neglected. This is especially true when $Da \gg 1$. In fact, in this case, chemical time scale is negligible with respect to the convective one.

In the study case, EDM model can be adopted within the combustion chamber, but it is not reliable in the nearby of the injection where convective time scale strongly varies and thus the Damköhler number. Moreover, EDM model should not be adopted into the nozzle, since it cannot predict evolution of species during the expansion.

By its nature, EDM model cannot be described by kinetic scheme. Only global reaction can be simulated. Ansys Fluent® provides the turbulence-chemistry interaction model due to Magnussen and Hjertager [3]. For methane/oxygen mixture, it provides two kinetic reaction models: mono-step model, characterized by one global reaction; two-steps model, a global reaction with one intermediate step. Furthermore, in [4], this method was applied to a *pseudo-reaction* mechanism, in which the completely detailed mechanism was reduced to only onestep, taking into account fuel-to-oxidizer ratio, specific combustion pressure, and chemical equilibrium composition calculated by means of minimization of Gibbs free energy.

2.3. Eddy-Dissipation Concept

As abovementioned, neither LFR nor EDM models can be accurate for the whole rocket combustion. Each one can be adopted only in small regions of fluid-dynamic volume. Moreover, EDM is limited by the lack of a kinetic mechanism. Ansys Fluent® provides an extension of EDM model to include detailed chemical mechanism in turbulent flows. It is a kind of fusion between LRF (for laminar fast flows) and EDM (for turbulent slow flows).

In the study case, since Damköhler number is not predictable, the EDC model is the best solution to implement. It can be used to describe the injection region, the combustion chamber, and the expansion (with exhaust plume outside the nozzle, as it will be described).

From a computational point of view, this model is the most expensive. It assumes that reaction occurs in small turbulent structures. Thus, the determination of these structures is very important for stability and stiffness of the iteration process.

3. Kinetic Scheme Reduction

Methane is the simplest thermodynamically stable hydrocarbon fuel possible.

However, its combustion is overall a very complex chemical phenomenon controlled by many physical processes including thermodynamics, buoyancy, chemical kinetics, radiation, mass and heat transfers and fluid mechanics. Several studies have focused on methane-air flames and now the oxidation of methane is quite well understood. Various kinetic mechanisms are reported in literature [5] and can be subdivided, with respect to considered reactions and species, into three fundamental classes:

- Detailed mechanisms;
- Skeletal mechanisms;
- Reduced mechanisms.

The detailed mechanisms are a very large set of elementary reactions up to hundreds of steps and involving dozens of chemical species including radicals. They describe with great accuracy the initiation, propagation, branching and termination of the oxidation reaction, but they are too heavy to be used in turbulent reacting flows CFD simulations, even though the CPU time and computer memory is continuously increasing.

Skeletal mechanisms are subsets of detailed mechanisms consisting always of elementary reactions, in which, for every combination of the operative conditions (temperature, pressure and composition), the unimportant chemical species are simply cancelled together with the associated reactions.

Several reduction methods are available mainly based on the Quasi Steady State Approximation (QSSA) and Partial Equilibrium (PE) assumptions.

Finally, reduced mechanisms are very small kinetic schemes consisting of less than ten non-elementary reactions involving tens of chemical species, in which the kinetic parameters and the reactions orders of all reactions are the results of a mathematical optimization process based on some available experimental data e.g., ignition delay times, adiabatic flame temperatures or flame speeds. Therefore, these schemes are applicable in the same narrow range of the operative conditions of the experiments used for the mathematical optimization procedure.

In the work here reported, a chemical technique was used for generation of skeletal, reduced kinetic schemes especially conceived for LRE applications. It consists of the following essential steps [6] [7]:

1. Identification of the most suitable detailed kinetic mechanism.
2. Selection of the relevant operative conditions i.e., initial temperature, pressure and composition.
3. Reaction path analysis.
4. Sensitivity analysis.

The system under investigation is a methane/oxygen LRE thrust chamber, operating at 52.5 bar. Therefore, a kinetic scheme developed for such extreme conditions, i.e., the RAM accelerator MECHANISM – RAMEC by Petersen and co-workers [8], was chosen as starting full mechanism.

Moreover, taking also into account that the combustion process in FSBB was started by means of an electric igniter heating the propellants in few milliseconds at a temperature greater than the auto-ignition point, the values reported in Table 1 were selected as initial operative conditions for the reduction process.

Table 1: Operative conditions selected for the reduction process

T [K]	P [bar]	ϕ
1000 – 1200	52.5	1

3.1. Reaction Path Analysis

This is a widely used method able to identify the unimportant chemical species and the corresponding reactions at certain operative conditions.

It consists in the determination through 0D chemical-kinetic simulations of an isothermal, isobaric, perfectly stirred reactor – PSR of the amount of chemical species containing a specified atom, in the present case, carbon, generated from a mole of methane. The calculation was carried out using the open-source Cantera [10] software under Python interface.

The net carbon element fluxes between chemical species j to k in a reaction r at an instance in time were evaluated according to the following relationship [11]:

$$\dot{C}_{rjk} = \frac{k_r n_{C,j} n_{C,k}}{N_{C,r}} \quad (2)$$

Where: k_r is the reaction rate, $n_{C,j}$ and $n_{C,k}$ are the numbers of carbon atoms in species j and k respectively and $N_{C,r}$ the total number of carbon atoms in the reaction r , for both reactants and products.

Summing all the element fluxes of carbon atom from species j to k , the total element flux is obtained:

$$\dot{C}_{jk}(t) = \sum_r \dot{C}_{rjk}(t) \quad (3)$$

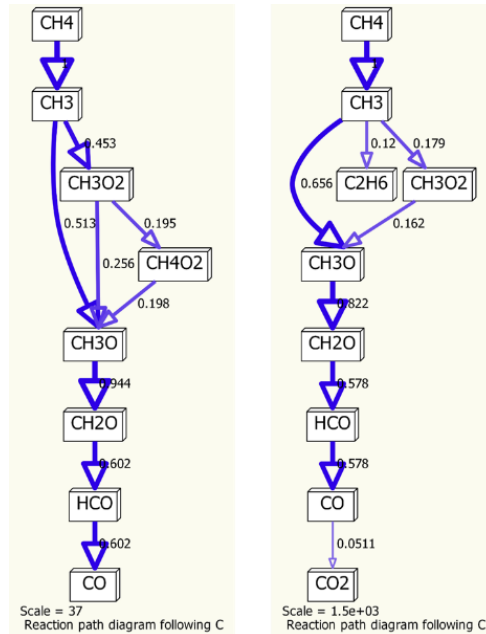


Figure 4. Reaction path diagrams following carbon atom of RAMEC mechanism at the operative conditions listed in Table 1. On the left at 1000 K and on the right at 1200 K

Finally, balancing all the in-flow and out-flow total element fluxes, following the carbon atom for every species in the kinetic mechanism, the reaction path diagram can be drawn, showing as nodes the chemical species and as arrows the element fluxes. For the RAMEC mechanism, at the operative conditions listed in Table 1 and setting a threshold on the value of the net element flux equal to 5%, the reaction path diagrams illustrated in Figure 4 were obtained.

These diagrams highlight the most relevant chemical species leading from reactants to products. Therefore, as the first step of the reduction process, the cancellation of all the species and the associated reactions of RAMEC scheme not reported in Figure 4 was performed.

Moreover, the reactions of the hydrogen/oxygen sub-mechanism, which is of fundamental importance for ignition, combustion and afterburning of methane, were also included.

In this way, an intermediate, reduced, skeletal, kinetic scheme containing only 20 species and 74 reactions was obtained.

3.2. Sensitivity Analysis

For progress on the reduction process, the suppression of the rate-limiting reactions at the selected operative conditions was carried out by means of calculation of the sensitivity coefficients S_r , using temperature as the control variable and the reaction rate k_r of every steps of the previous intermediate mechanism, arising from the reaction path analysis. Sensitivity coefficients were therefore evaluated by PSR simulation at 1200 K, in agreement with the following relationship:

$$S_r = \frac{k_r}{T} \frac{\partial T}{\partial k_r} \quad (4)$$

All reactions with $|S_r| < 10^{-5}$ were neglected. Then, coefficients were normalized with the maximum S_r value. The largest ones were reported in Figure 5.

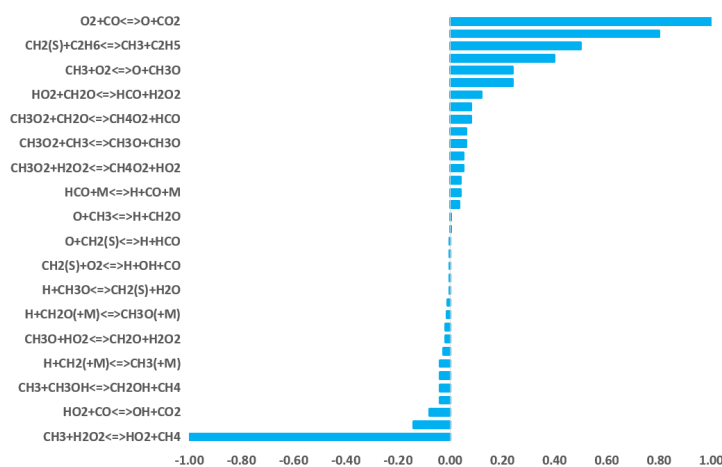


Figure 5. Largest normalized sensitivity coefficients for PSR at 1200 K

Finally, the CIRA High Pressure Rocket Burn – HPRB reduced, skeletal, kinetic scheme consisting in 18 species and 47 reactions was derived.

A preliminary assessment of this methodology was carried out using two further reduced, skeletal, kinetic mechanisms, denominated respectively Low Pressure Rocket Burn – LPRB and Medium Pressure Rocket Burn – MPRB, generated with the same abovementioned technique [12]. Both of them were derived starting from Lu 30 detailed scheme [13], which, in turn, was a reduced version of GRI-Mech 3.0 [14] and using the operative conditions summarized in Table 2.

LPRB, containing 16 chemical species and 48 elementary reactions, was generated at atmospheric pressure, especially for modelling methane/oxygen afterburning in the exhaust plume from a rocket nozzle. MPRB, including 18 species and 50 reactions, was instead developed at intermediate-high pressure, above all for rebuilding the single-injector combustion chamber experiments, conducted at the University of Munich [15].

Table 2: Operative conditions selected for development of LPRB and MPRB

	T [K]	P [bar]	ϕ
LPRB	2000	1	1
MPRB	1200 - 1500	20	2.6

4. FSBB Test Campaign

As abovementioned, FSBB test-article is functionally equivalent to HYPROB-NEW final demonstrator (DEMO), except for the cooling jacket. Thus, experimental data obtained by FSBB firing-tests are completely suitable for HPRB kinetic scheme validation, which is obtained for DEMO condition. A dedicated test-campaign was carried out at ASI/AVIO FAST2 facility in Colleferro (RM-Italy) [16]. This campaign consisted of several runs, using an incremental approach for what concerns objective chamber pressure. Thus, starting from a low combustion pressure of about 31 bar (corresponding to about 12 kN of thrust) for the first trial, we reached more than 48 bar (nearly 20 kN) in the last one (see Figure 6).

The test-article was fed by high-pressure vessels: cryogenic tank for oxygen, while ambient temperature tank for methane. Calibrated orifices were adopted in order to obtain desired mass-flow rate.



Figure 6: FSBB firing-test. Test06 (48.51 bar)

Pressure signals were acquired during firing-tests and analysed in order to obtain the steady-state value (Figure 7). These values will be compared to CFD predictions so that transient phases can be neglected. In this way, stationary CFD simulation can be used for comparison.

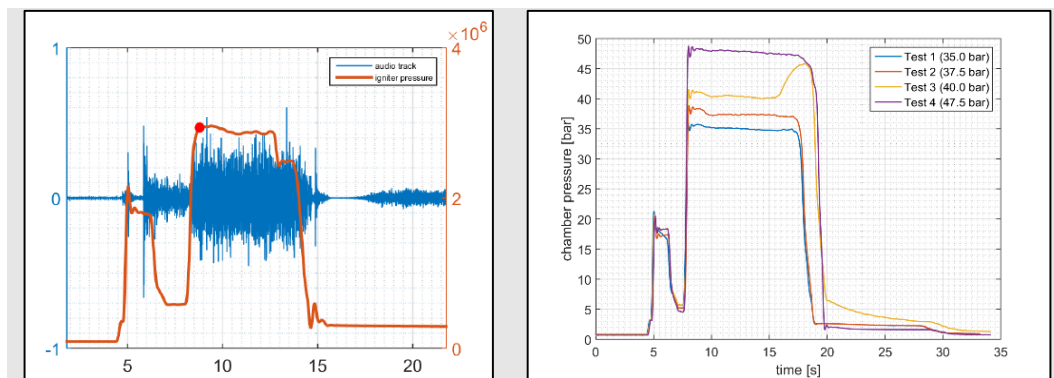


Figure 7: Chamber pressure signal analysis (left) and chamber pressure comparison for several tests

It was possible to extract fluid-dynamic structures of exhaust plume using image information collected by high-resolution video acquisition. In Figure 8, the luminance information of the image is reported. This was obtained by performing a pixel-to-pixel subtraction. The resulting image will be used for a qualitative comparison on CFD simulation of exhaust plume.

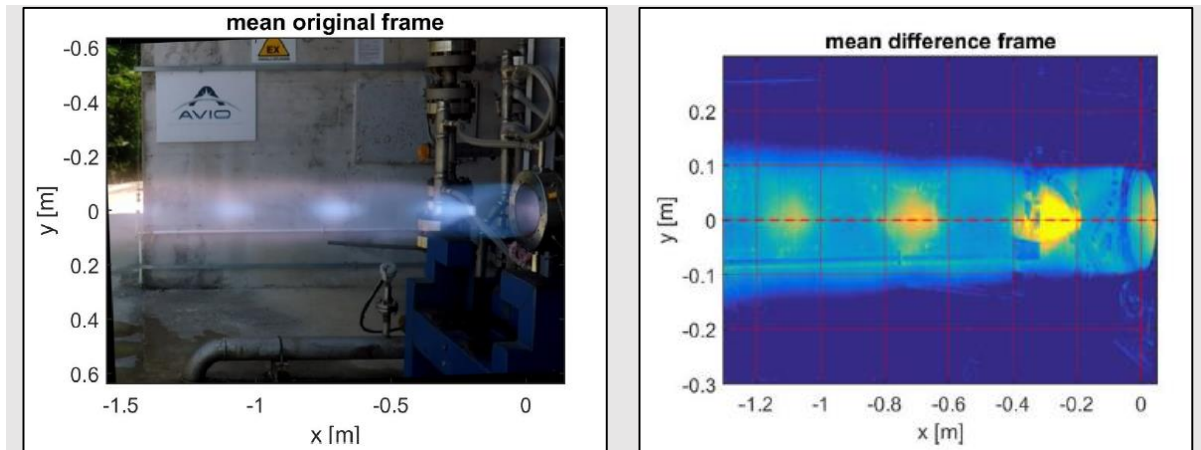


Figure 8: Single frame extracted from video acquisition, in true colour (left) and false colour (right)

4.1. Experiment Results

In Table 3, all data collected during the test campaign are reported. In particular, in this work, the last firing-test (named TEST06) is selected for CFD comparison. This was performed at highest pressure during the campaign and the pressure reached is the closest to the design one of the final demonstrator (52.5 bar). Moreover, also TEST04 will be adopted for comparison, since it was performed at almost nominal mixture ratio (w.r.t. DEMO design).

In order to correctly simulate test condition, the following data will be applied from the test result table:

- Measured pressure and temperature of methane;
- Measured pressure and temperature of oxygen;
- Measured mass-flow rate of methane;
- Extrapolated mass-flow rate of oxygen (from pressure drop);

Table 3: Data collection of entire FSBB test-campaign

Property	TEST04	TEST06	DEMO (design)
Combustion Chamber Pressure [bar]	39.92	48.51	52.5
Mixture Ratio	3.41	3.21	3.4
Specific Impulse [s]	250.50	260.52	280

5. Kinect Schemes CFD validation

Preliminarily, LPRB and MPRB kinetic schemes were compared with most common used kinetic schemes. This enabled us to develop the method adopted for HPRB derivation. In particular, CFD simulation regarding the expansion of hot gases from nozzle towards the ambient pressure was considered. The problem was simply described by 2D axis-symmetric computational domain. The domain is constituted by nozzle (convergent-divergent) and ambient volume. The mesh type is structured and it is made of 100k nodes. The turbulence model is $k - \omega$ model, since it is y^+ insensitive. In addition, SST (shear-stress transport) option was enabled, and initial height of 0.01mm at walls was set. For cell growing, ratio 1.2 was used. In Figure 9, details on computational domain are reported.

The injection was not simulated in this case. To determine the mixture composition inside the combustion chamber (just before the expansion through the nozzle), RPA tool was adopted [17]. This tool, starting from geometry parameters and injection ones, reveals the mixture composition obtained by Gibbs Free Energy Minimization, in the hypothesis of evolving equilibrium. RPA tool was previously validated using experimental measures obtained during test campaign.

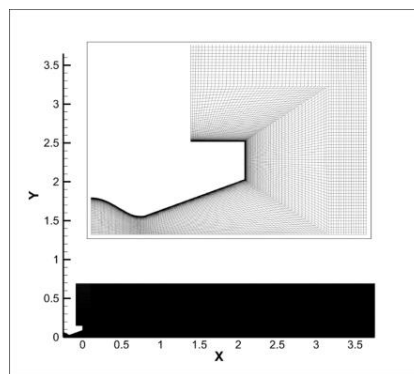


Figure 9: Detail of 2D axis-symmetric structured-mesh domain

In order to have a reliable reference for chemical reaction, the most used schemes were selected:

- **GRI-Mech 3.0.** This mechanism is due to Gas Research Institute [14]. This scheme is intended for combustion involving any hydrocarbon, thus also for methane. It is the most accurate, and therefore also reliable, kinetic scheme. It is constituted by 53 species and 325 reactions. Since it is a complete scheme, it is also the most expensive from a computational point of view. It will be used as reference.
- **REDRAM.** This is a skeletal kinetic mechanism. The mechanism has been intended for the modelling of methane ignition at RAM accelerator conditions, which means the pressures above 40 atm. The mechanism was derived from a detailed mechanism of the same research group. The detailed mechanism called RAMEC was obtained from an earlier version of the GRI-Mechanism by adding the reactions of peroxy species: CH_3O_2 , $\text{CH}_3\text{O}_2\text{H}$, $\text{C}_2\text{H}_5\text{O}$, $\text{C}_2\text{H}_5\text{O}_2$, and $\text{C}_2\text{H}_5\text{O}_2\text{H}$. The addition of the kinetics of peroxy species improved significantly the agreement of RAMEC with experimental data at high pressures. The reduced (skeletal) mechanism was derived by Petersen and Hanson [9] from RAMEC by systematically eliminating reactions and species that have no influence on the ignition delay time or on the final product temperature. This scheme is constituted by 22 species and only 34 reactions. For this reason, it is the simplest among the ones considered.
- **KONG.** In order to improve prediction of REDRAM, Zhukov and Kong [18] proposed another skeletal scheme, with 23 species and raising to 49 reactions. Results confirmed that KONG scheme gives concentrations very close to GRI3.0 prediction, despite slight number of species and reaction (if compared to GRI3.0).

In Figure 10, the contour-plot of Mach number is reported as comparison of the abovementioned kinetic schemes. As can be seen, from a qualitative point of view, results are quite similar. Mach diamonds are predicted in every simulation at the same distance from the nozzle outlet.

For the sake of clarity, in Figure 11 a comparison between acquired image during firing-test TEST06 and CFD results obtained by adoption of GRI-Mech 3.0 mechanism is reported. The fluid-dynamic structures are quite similar and Mach diamonds locations are well predicted. The exhaust plume is a peculiar region to evaluate chemical reactions, since it is characterized by a wide range of convective scales. Thus, it justifies the adoption of EDC model.

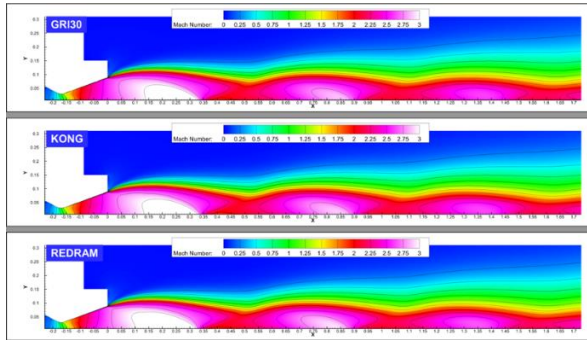


Figure 10: Mach number contour-plots. Most used kinetic schemes comparison. (TEST06 simulation)

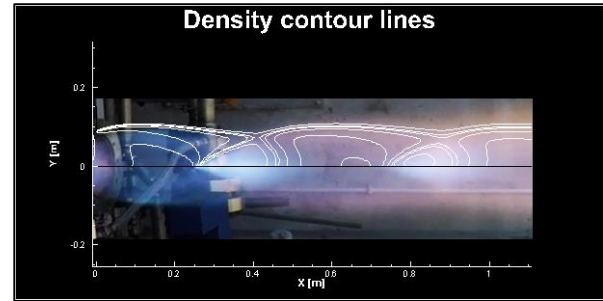


Figure 11: Qualitative comparison. Density contour lines. TEST06. GRI3.0

In Figure 12, temperature is compared using abovementioned schemes and new ones proposed in section 3. As can be seen, results are quite similar and could justify the adoption of a skeletal mechanism when GRI3.0 is not suitable. Moreover, in Figure 13, a comparison of speed-up in execution time is reported. Values are calculated for single iteration in each CFD run, using the same mesh, boundary condition, models and setup. Results are reported in Figure 12. Thus, adopting GRI3.0 as reference unit, KONG scheme is 2.76 times faster and LPRB is 3.71 times faster. HPRB model (derived for high pressure involved in combustion chamber) will be used below.

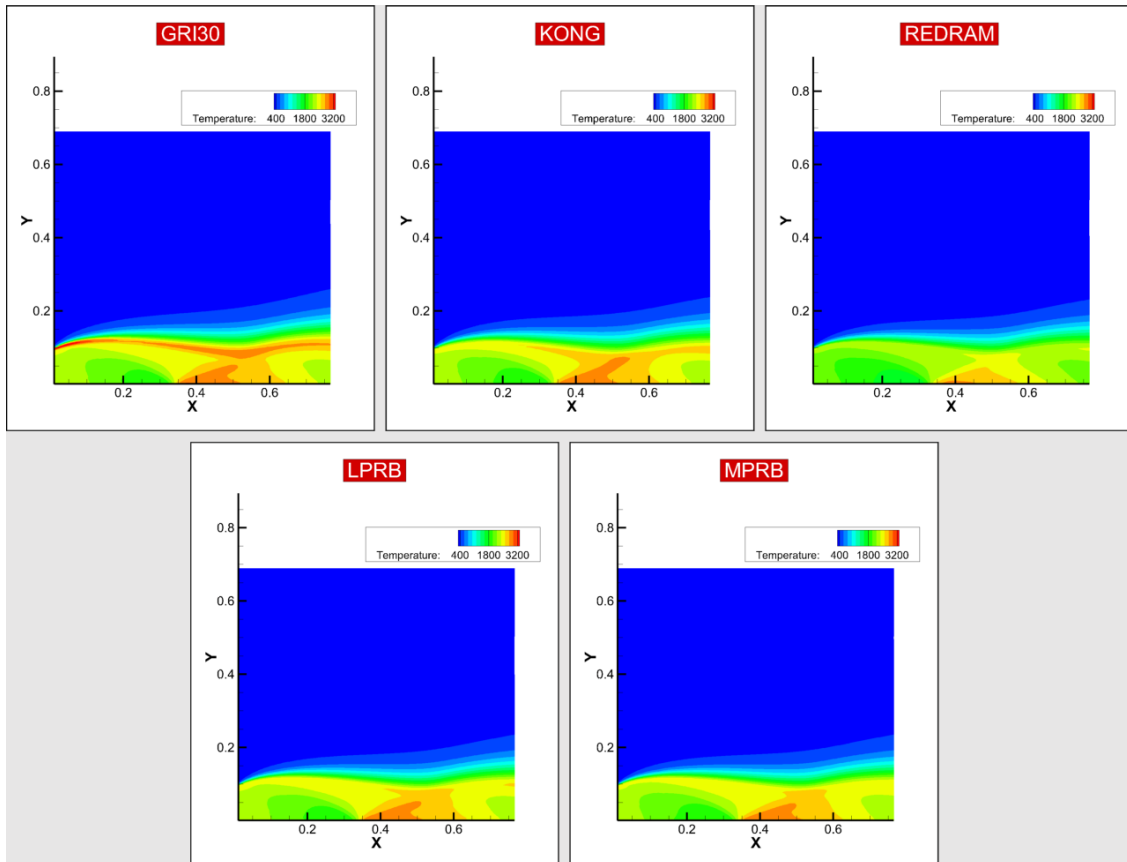


Figure 12: Temperature contour-plot comparison. TEST06 condition.

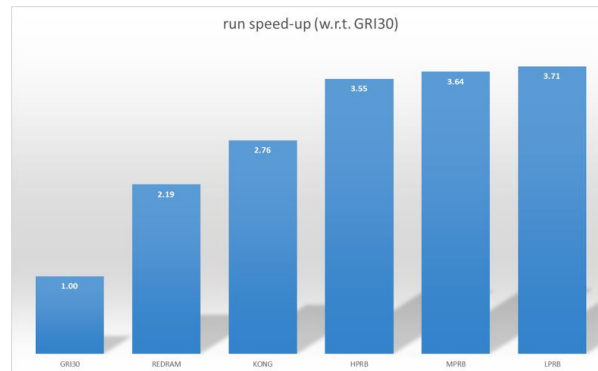


Figure 13: Speed-up rate

5.1. FSBB Firing-Test CFD Rebuild

In these cases, for a good spatial description, a huge number of cells was needed and adoption of complete kinetic scheme led to prohibitive computational costs. In Figure 14 the geometry selected to perform simulations is reported. This is complicated by injector shape and firing plate design (green). It is not possible to accurately represent fluid-dynamics by 2D simplification, thus only 3D mesh could be adopted. On the other hand, taking advantage of rotational periodicity, only a 60°-wide wedge has been extracted, assuming symmetry boundary condition on slices.

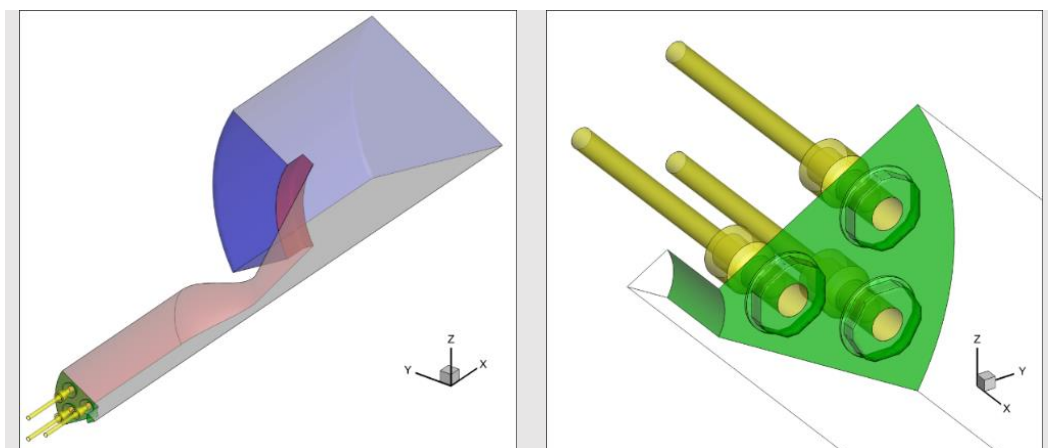


Figure 14: FSBB geometry adopted for 3D CFD simulation. Overall view (left) and firing-plate detail (right).

In Figure 14: red, internal wall of combustion chamber and nozzle (where heat-fluxes stand on); green, firing-plate (facing combustion flames); yellow, injector walls (methane and oxygen).

Due to the complexity of the geometry, only unstructured meshes have been drawn with a very high number of cells. Three meshes have been created, with different densities.

- Low density mesh with 2'855'757 cells (named L);
- High density mesh with 12'173'422 cells (named H);
- Very high density mesh with 53'176'759 cells (named V).

In Figure 15, comparisons of heat fluxes, standing on the combustion chamber, are reported for the three mesh density levels. As can be seen, they demonstrate a good mesh convergence, justifying the adoption of lower density meshes for comparison. For the sake of simplicity, these results were obtained implementing EDM method for chemical reactions with a simple dual-step kinetic scheme.

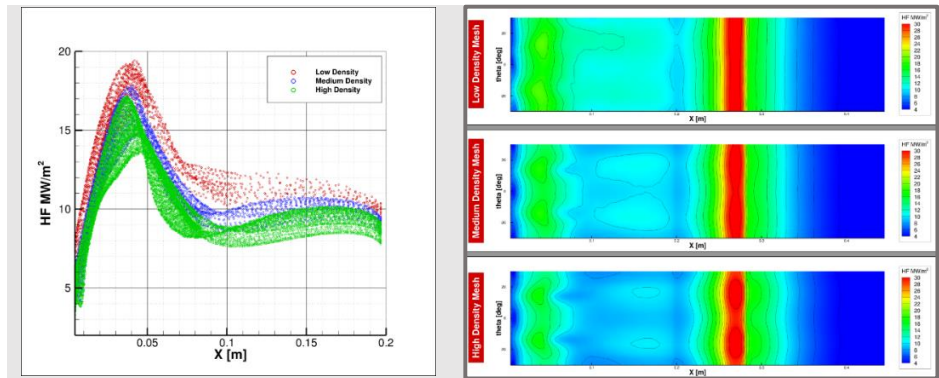


Figure 15: Mesh convergence analysis. Punctual heat-flux standing on combustion chamber (on right); heat-flux contour-plot over rectified internal wall (cylindrical coordinates) CC+Nozzle

5.2. CFD Results comparison

Hereinafter, CFD results will be reported comparing them, when available, with experimental values. In following keys, 2S denotes dual-step methane/oxygen kinetic model (with EDM), while HPRB denotes methane oxidation kinetic scheme proposed in this work (with EDC). It is immediately evident that the higher heat flux is obtained by HPRB. It is necessary to take into account that, for these simulations, the boundary condition on the wall is a “constant temperature” of 500 K. Thus, the calculated heat-fluxes could be not dimensional and had to be scaled with actual wall temperature (not available from experiment). In any case, the validity of the comparison was preserved, since all simulations were carried out in the same conditions. In order to verify mesh density insensitivity, low density (L) and medium density (H) are reported for HPRB.

As can be seen in Figure 16, the pressure calculated by means of HPRB is significantly higher than experimental measurement. This can be explained by incorrect oxygen mass-flow rate. In fact, this mass-flow rate is not experimentally “measured” but extrapolated by pressure-drop measurement. Since oxygen is in cryogenic status, a slight temperature change could lead to high density change, affecting the calculated mass-flow rate value. For this reason, the experimental value should be further investigated.

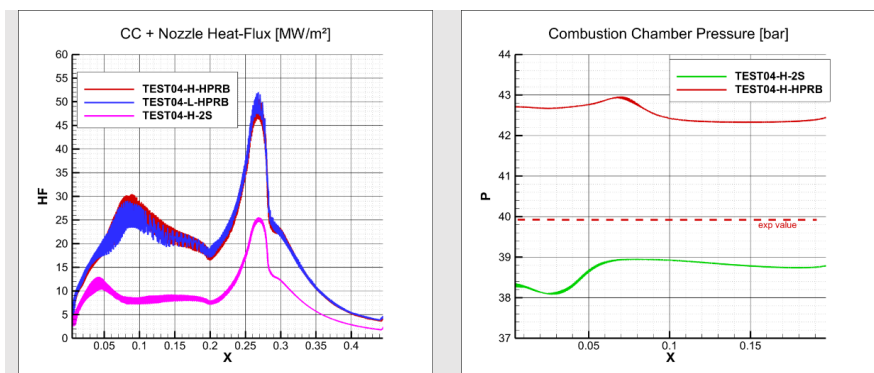


Figure 16: TEST04 results comparison. On the left, heat fluxes standing on combustion chamber and nozzle. On the right, pressure distribution on combustion chamber

In Figure 17, the same results are reported for TEST06. In this case, the pressure value is close enough to the experimental one. Even if HPRB result is slightly higher than the experimental reference, the value is better than 2S one. Meanwhile, heat-flux result confirms to be higher than dual-step calculation. The under-estimation of the dual-step model, on both pressure and heat-fluxes, can be easily explained: since this simple model cannot describe detailed combustion, adiabatic temperature, gas mixture composition, and subsequently partial pressures, are not captured. Therefore, heat-flux, which strictly depends on adiabatic temperature, is wrong and total pressure, due to partial pressures and total temperature.

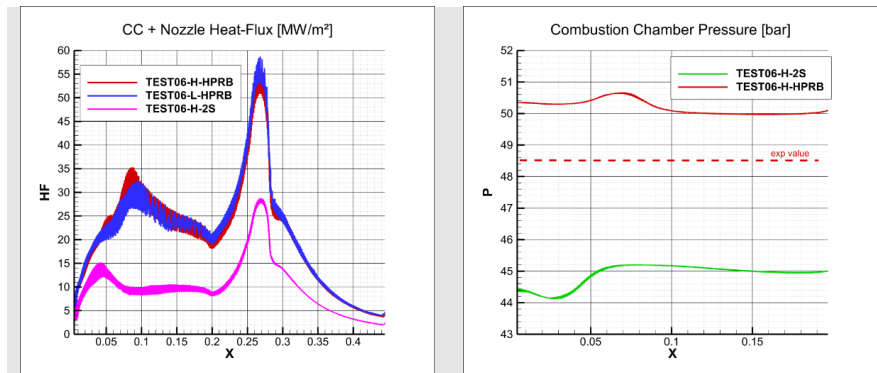


Figure 17: TEST06 results comparison.

In Figure 18, results for DEMO conditions are compared. In this case, no experimental data are available. Nevertheless, design value for pressure is reported as reference for chamber pressure. As can be seen, the value predicted by HPRB model is exactly in line with prediction. This validates HPRB model and confirms what abovementioned: the over-estimation in the previous chamber pressure value (for cases TEST04 and TEST06) could be addressed by wrong mass-flow rate interpretation and need further experimental analysis. For heat-flux, similar considerations can be drawn: values obtained by means of HPRB model are significantly higher than the 2S ones. For the sake of comparison, three mesh density levels are reported for 2S model, confirming again the mesh convergence.

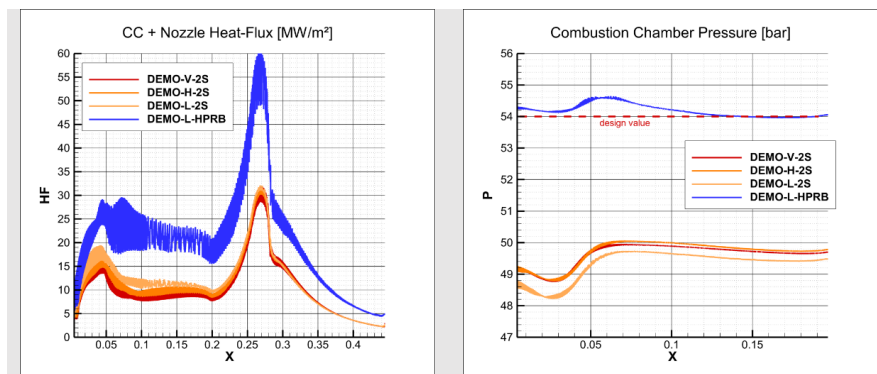


Figure 18: DEMO results comparison. No experimental data is available.

In Figure 19, the firing plate is shown. The picture is taken after the test campaign completion (after TEST06). Some blackening regions are clearly visible. Black areas are concentrated in the nearby of the igniter (hole in the centre) and just outside injectors (in particular, inner channel). This phenomenon is probably ascribed to heating due to the peculiar flame shape and fluid-dynamic pattern.



Figure 19: Firing-Plate after test campaign completion

In Figure 20, CFD results are reported. On the left, results obtained in DEMO conditions are illustrated. In this plot, the three mesh density levels are reported for dual step chemical model (2S). As it can be deduced, solution obtained by low-density mesh (DEMO-L-2S) is slightly asymmetrical, while the densest (DEMO-V-2S) is perfectly symmetrical. Nevertheless, overall distribution values are quite similar. For this reason, comparison with the solution HPRB obtained with low-density mesh can be reasonable.

On the right hand of Figure 20, CFD results in TEST04 conditions (left) and TEST06 conditions (right) are depicted, comparing HPRB model with dual-step. For both tests, HPRB predicts an over-heating region exactly where found in the previous picture (Figure 19). Moreover, the overheating region around injectors (green colour in plots) seems to be bridged, as the picture can confirm (copper colour is homogeneous in the same region). On the contrary, a simple dual-step model cannot predict this phenomenon. In fact, dual-step is based on EDM method, which cannot describe detailed combustion. Thus, gas composition is incorrect and, subsequently, inertia of mixture, affecting the fluid dynamics involved. Neither bridging regions are predicted by 2S, neither overheating around igniter nor inner injectors.

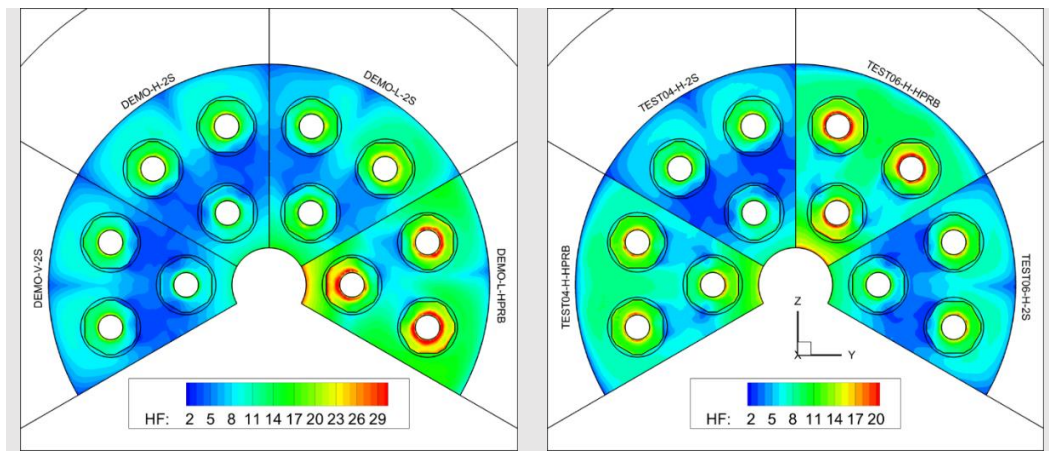


Figure 20: DEMO (on left) and experiments TEST04 and TEST06 (on right) comparison. Heat-flux contour-plots on firing-plate.

In Figure 21, contour plot of temperature is reported on middle plane slice, crossing the combustion chamber. Within each of the four frames, on the left, the injector can be distinguished by the low temperature (of propellants), while, on the right, ambient volume is visible. It is clearly visible that flames obtained by 2S and HPRB are different not only in temperature but in shape. In case of HPRB, flame is closer to the combustion chamber wall, justifying higher heat-fluxes calculated by this model.

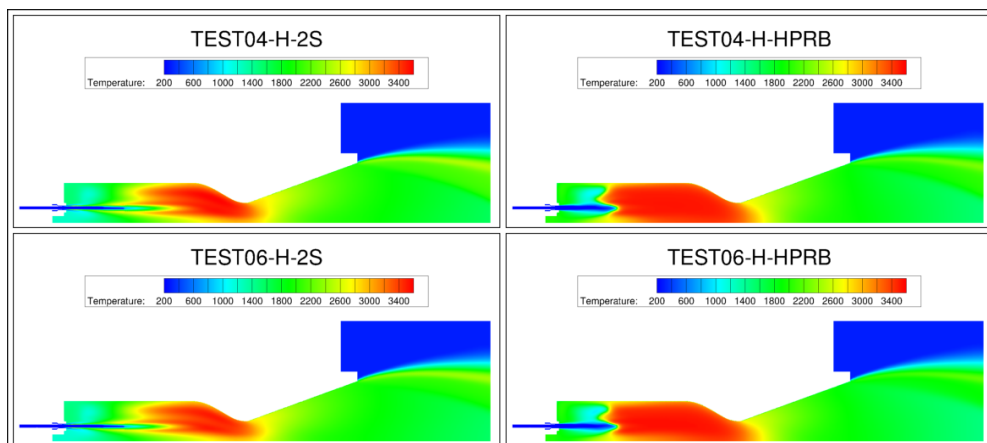


Figure 21: Temperature comparison on middle plane

6. Conclusions

In the last years, there has been a growing interest in methane oxidation models. This is because, if on one hand full schemes proved too expensive from a computational point of view, becoming prohibitive in some cases, on the other hand simplified kinetic scheme revealed to be not accurate enough to describe phenomena involved in combustion.

In this work, a new skeletal kinetic scheme for methane/oxygen combustion has been proposed, named HPRB. The mechanism was developed from RAMEC mechanism, which is the most reliable for methane high-pressure combustion. To obtain skeletal mechanism, a reduction was carried out using reaction-path and sensitivity analyses method. 2D axis-symmetric simulations have proven the scheme is more than 3.5 times faster than GRI-Mech 3.0 (Figure 13).

Subsequently, the scheme was used for CFD test rebuilding of FSBB test-campaign (in the framework of HYPROB program). Comparing results with experimental data collected during the campaign, it confirmed to be more reliable than the previously used dual-step method.

Nevertheless, HPRB scheme is valid only in the conditions in which it is applied (DEMO). More specifically, it is obtained for the specific mixture-ratio and combustion chamber pressure range. Moreover, all simulations here presented are obtained using the ideal gas model. While this assumption is valid in the combustion chamber, where high temperatures are involved, it could not be valid through the injection zone, where propellant temperatures are relatively low and fluids exhibits non-ideal behaviour. In addition, in order to verify the of the reliability of predicted heat-fluxes, a dedicated test-campaign should be carried out, so that applied wall temperature in simulation could be more accurate and predictive.

For this aim, during further HYPROB-NEW activities, a new dedicated firing-test campaign will be carried out on windowed test-articles. In those cases, it will be possible to acquire experimental data on flame temperature, mixture composition and, if possible, heat-fluxes standing on chamber wall. When those data are available, HPRB kinetic scheme will be further validated.

7. Acknowledgements

This work has been carried out within the HYPROB-NEW project, funded by the Italian Ministry of University and Research (MIUR) whose financial support is much appreciated.

8. References

- [1]. F. Battista, et al., Hyprob Project: Status of the Technological and Experimental Activities of the LRE Development Line, *Space Propulsion, Seville, Spain, 2018*.
- [2]. F. Battista et al., Technological Advancements in the HYPROB Project - Demonstrators Development Line, *International Astronautical Conference (IAC) 2018, Bremen (Germany)*
- [3]. B. F. Magnussen and B. H. Hjertager, On Mathematical Models of Turbulent Combustion with Special Emphasis on Soot Formation and Combustion. In *16th Symp. (Int'l.) on Combustion. The Combustion Institute, 1976*.
- [4]. G. Saccone, P. Natale, F. Battista, P. Breda, M. Pfitzner, Methane/Oxygen Combustion Kinetic Scheme Optimization for Liquid Rocket Engine CFD Applications, Proceedings of the 4th World Congress on Momentum, Heat and Mass Transfer (MHMT'19), Rome, Italy – April 2019.
- [5]. Guessab, A.; Aris, A.; Bounif, A.; 2013, Simulation of Turbulent Piloted Methane Non-Premixed Flame Based on Combination of Finite-Rate/Eddy-Dissipation Model, *Mechanika 19(6)*, 657-664.
- [6]. Tomlin, A.S.; Turanyi T.; Pilling, M.J. Low-Temperature Combustion and Autoignition, Comprehensive Chemical Kinetics; Compton, R.G.; Hancock, G., Eds., Elsevier 1997; Vol. 35, Chapter 4, 293-437.
- [7]. A. Saylam, M. Ribaucour, W.J. Pitz, R. Minetti (2006), Reduction of Large Detailed Chemical Kinetic Mechanisms for Autoignition Using Joint Analyses of Reaction Rates and Sensitivities, *International Journal of Chemical Kinetics*.
- [8]. E.L. Petersen, D.F. Davidson, R.K. Hanson, Kinetics Modeling of Shock-Induced Ignition in Low-Dilution CH₄/O₂ Mixtures at High Pressures and Intermediate Temperatures, *Combustion and Flame, Vol. 117, pp. 272-290 (1999)*.
- [9]. E. Petersen, R. K. Hanson, Reduced Kinetics Mechanisms for Ram Accelerator Combustion, in *Journal of Propulsion and Power, 15, 1999, pp. 591-600*.
- [10]. D. Goodwin, H. K. Moffat, R. L. Speth. (2017). Cantera: An Object-oriented Software Toolkit for Chemical Kinetics, Thermodynamics, and Transport Processes (2.6 version) [Online]. Available: <http://www.cantera.org>.

- [11]. Revel, J. and Boettner, J.C. and Cathonnet, M. and Bachman, J.S. Derivation of a Global Chemical Kinetic Mechanism for Methane Ignition and Combustion. *Journal De Chimie Physique et De Physico-Chimie Biologique*, 91(4): 365(382, April 1994. ISSN 0021-7689.
- [12]. P. Natale, G. Saccone, A. French, F. Battista, Chemical and CFD modeling of Sub-Scale Bread-Board igniter based on experimental data assessment, *51st AIAA/ASME/SAE/ASEE Joint Propulsion Conference, 27-29th July, 2015, Orlando, Florida*.
- [13]. T. Lu, C. K. Law, C. S. Yoo, J. H. Chen, Dynamic Stiffness Removal for Direct Numerical Simulations, in *Combustion and Flame*, 156, 2009, pp. 1542-1551.
- [14]. Gregory P. Smith, David M. Golden, Michael Frenklach, Nigel W. Moriarty, Boris Eiteneer, Mikhail Goldenberg, C. Thomas Bowman, Ronald K. Hanson, Soonho Song, William C. Gardiner, Jr., Vitali V. Lissianski, and Zhiwei Q in http://www.me.berkeley.edu/gri_mech/
- [15]. M. P. Celano, S. Silvestri, G. Schlieben, C. Kirchberger, O. J. Haidn and S. Menon, Injector Characterization for a Gaseous Oxygen-Methane Single Element Combustion Chamber, in *Progress in Propulsion and Power*, Vol. 8, 2016, pp. 145-164.
- [16]. F. Battista et al., The HYPROB LOX-LCH4 Demonstrator: Status of the Manufacturing and Experimental Activities, *7TH European Conference for Aeronautics and Space Sciences 2017, Milan (Italy)*
- [17]. Rocket Propulsion Analysis, by Alexander Ponomarenko. <http://propulsion-analysis.com/about.htm>
- [18]. Victor P. Zhukov and Alan F. Kong, Skeletal Kinetic Mechanism of Methane Oxidation for High Pressures and Temperatures, *7th European Conference for Aeronautics and Space Sciences (EUCASS) 2017, Milan (Italy)*